Isotope effects in resonant two-color photoionization of Xe in the region of the $5p^5(^2P_{1/2})4f[5/2]_2$ autoionizing state

2015 New J. Phys. 17 043054

(http://iopscience.iop.org/1367-2630/17/4/043054)

New Journal of Physics
The open access journal at the forefront of physics

Deutsche Physikalische Gesellschaft DPG
IOP Institute of Physics

Published in partnership with: Deutsche Physikalische Gesellschaft and the Institute of Physics

OPEN ACCESS

RECEIVED
20 November 2014

REVISED
9 March 2015

ACCEPTED FOR PUBLICATION
24 March 2015

PUBLISHED
27 April 2015

PAPER

Isotope effects in resonant two-color photoionization of Xe in the region of the $5p^5(^2P_{1/2})4f\,[5/2]_2$ autoionizing state

E V Gryzlova[1], P O'Keeffe[2], D Cubaynes[3,4], G A Garcia[4], L Nahon[4], A N Grum-Grzhimailo[1] and M Meyer[5]

[1] Skobeltsyn Institute of Nuclear Physics, Lomonosov Moscow State University, Moscow 119991, Russia
[2] CNR-ISM Istituto di Struttura della Materia, CP10, I-00016 Monterotondo Scalo, Italy
[3] ISMO, CNRS / Université Paris-Sud, Bâtiment 350, F-91405 Orsay Cedex, France
[4] Synchrotron SOLEIL, L'Orme des Merisiers, St Aubin, B.P. 48, F-91192 Gif sur Yvette, France
[5] European XFEL GmbH, Albert-Einstein-Ring 19, D-22761 Hamburg, Germany

E-mail: gryzlova@gmail.com

Keywords: photoionization, isotopes, photoelectron angular distribution

Abstract

Isotope effects in two-photon two-color photoionization are investigated by a combined theoretical and experimental study of the ionization of xenon atoms. A combination of variable polarization synchrotron and laser radiations are used to excite the $5p^5\,(^2P_{1/2})\,4f\,[\frac{5}{2}]_2$ autoionizing resonance via the intermediate $5p^5\,(^2P_{3/2})\,5d\,[\frac{3}{2}]_1$ state. Electrons and ions are detected in coincidence in order to extract the photoelectron angular distributions and the values of the linear and circular dichroism and to determine how these depend on the isotope. A complete theoretical model of the two-photon process in atoms is given in order to describe these parameters as a function of the polarization of the exciting light sources (both linear and circular polarization). Furthermore, the hyperfine depolarization due to the coupling of the electronic and nuclear angular momenta in the intermediate state is taken into account. The results of the theoretical model are in agreement with the experimental results and allow estimation of the previously unknown hyperfine structure (HFS) constant for the case of overlapping HFS levels.

1. Introduction

The measurement of photoelectron angular distributions (PADs) and dichroic effects in two-color experiments is a widely used method to access detailed information on the electronic dynamics going on during a photoionization process [1, 2]. The purpose of performing a two-photon experiment is to allow the target to be prepared in a well defined state, including orientation/alignment of its angular momentum vector. In this way the PAD formed on absorption of a second photon contains more valuable information on the photoionization dynamics with respect to that obtained in single photon ionization. Measurements of the relative intensities of the photoionization signal while changing the two polarization states of the first and second photon fields (linear and circular dichroism (CD)) provides additional experimental parameters which can be measured to describe the process.

This ideal situation is complicated in the case of atoms with nonzero nuclear spin. It has long been recognized that carefully prepared aligned states suffer from a depolarization effect due to coupling of the total electronic angular momentum $\mathbf{J}$ with that of the nucleus $\mathbf{I}$. In spite of the small relative size of the nuclear magnetic moment, which leads to very small modifications of the energy levels (hyperfine splittings), the effect on the multipole moments of an aligned/oriented electronic angular momentum ensemble can be very large due to the precession of the total electronic angular momentum about the new total angular momentum, $\mathbf{F} = \mathbf{I} + \mathbf{J}$. Indeed, if a pulsed excitation source excites, in a coherent manner, a number of hyperfine states, this precession can be observed in the form of quantum beats in the fluorescence decay of the state as observed experimentally

by Haroche *et al* [3] for Cs atoms. The time evolution of the alignment of the angular momentum was then analyzed from a theoretical point of view by Fano and Macek [4] and by Greene and Zare [5].

The effect of this coupling on the PADs of the electrons emitted from aligned intermediate states was observed and discussed in a series of works by Berry and coworkers [6–9] concentrating on the effect of hyperfine coupling on the PADs in multiphoton ionization of alkali and alkaline earth atoms. It was also noted that the use of nanosecond [10] or microsecond [11] lasers lead to different PADs in the multiphoton ionization of Cs through the $7P_{3/2}$ state. These differences were found to be due to different temporal averaging of the hyperfine depolarization [10].

Therefore, it is clear that a complete understanding of the multiphoton PADs in atoms with nonzero nuclear spin requires the ability to perform isotopically resolved experiments in order to obtain a detailed knowledge of this depolarization effect. One way to access the different photoionization dynamics of the individual isotopes is given by ultra-high resolution spectroscopy (e.g. [12]).

Another approach was used by the present authors in a recent study [13], where they applied a photoelectron imaging/photoion coincidence technique. In the two-color photoionization of Xe atoms, selection of isotopes with a zero nuclear spin $I = 0$ (^{132,134,136}Xe) allowed isolating the pure electronic dynamics in the photoionization process by extracting PADs, linear dichroism (LD) and CD associated with the $I = 0$ atoms. Xenon is an ideal case for isotopically resolved studies as the natural isotope mixture of Xe consists of approximately 26% of the isotope ^{129}Xe with nuclear spin $I = \frac{1}{2}$, 21% of ^{131}Xe with $I = \frac{3}{2}$, while the other isotopes have vanishing nuclear spin. Other prominent examples of atoms with significant natural isotope populations with both $I = 0$ and $I \neq 0$ include Kr, Ba and Sr. The two-photon transition examined in xenon provided a case of complex photoionization dynamics on which to fully test the technique. In the first step, the atom is excited by the photon $\hbar\omega_1$

$$\hbar\omega_1 \; + \; \mathrm{Xe}\left(5p^6\right) \rightarrow \mathrm{Xe}^{\star}\left(5p^5\,{}^2P_{3/2}5d\,[3/2]_1\right). \tag{1}$$

Then, the excited atom is further excited by the photon $\hbar\omega_2$, followed by autoionizing decay and emission of the photoelectron e^-_{ph},

$$\begin{aligned}\hbar\omega_2 \; + \mathrm{Xe}^{\star}\left(5p^5\,{}^2P_{3/2}5d\,[3/2]_1\right) &\rightarrow \mathrm{Xe}^{\star}\left(5p^5\,{}^2P_{1/2}\right)4f\,[5/2]_2, \\ &\rightarrow \mathrm{Xe}^{+}\left(5p^5\,{}^2P_{3/2}\right) + e^-_{\mathrm{ph}}(lj).\end{aligned} \tag{2}$$

In the jK-coupling scheme, the $\mathrm{nl}\,[\mathrm{K}]_\mathrm{J}$ indicates, for the Xe atom, that the total angular momentum $\mathbf{j}$ of the $5p^5_j$ core is first coupled to the orbital momentum of the excited electron $\mathbf{l}$, $\mathbf{j} + \mathbf{l} = \mathbf{K}$, with subsequent coupling of the spin of this electron, $\mathbf{K} + \mathbf{s} = \mathbf{J}$. Primed and not primed orbitals of the excited electron correspond to $j = \frac{1}{2}$ and $j = \frac{3}{2}$, respectively. The emitted electron is described by orbital (l) and total (j) angular momenta. Here the large number of open channels (eight in total) and the variation of the interaction between the direct and autoionization channels (Fano profile) while tuning the laser across the $5d\,[\frac{3}{2}]_1 \rightarrow 4f'\,[\frac{5}{2}]_2$ resonance provides us with the opportunity to fully test the comparison of theory and the experimental results.

In the first work [13] only the PADs from a geometry involving parallel linear polarizations of $\hbar\omega_1$ and $\hbar\omega_2$ for the $I = 0$ atoms were considered. Here we provide the theoretical framework to describe the PADs and dichroic effects for isotopes with nonzero nuclear spin and provide further comparison with experimental data for both circularly and linearly polarized radiation beams. Furthermore, we examine the differences between the PADs for isotopes with different I in order to see if it is feasible to use the measurements of the PADs to provide information on the hyperfine interaction in the intermediate state, and extract a previously unknown (relative) hyperfine constant.

The structure of the paper is as follows: in section 2 the experimental set-up is described in a detailed fashion; in section 3 the description of the theoretical framework used to calculate the PADs and the dichroic effects is given; and in section 4 the isotope effect on the dichroism and PADs is discussed by comparing the experimentally measured values with the calculated parameters.

2. Experiment

The isotopically resolved photoelectron imaging two-color experiment is the same as that discussed in the recent study [13] and is schematically illustrated in figure 1. The experiments were performed at the VUV beamline, DESIRS [14], of the French synchrotron source, SOLEIL, together with the permanently installed molecular beam chamber SAPHIRS.

A supersonic beam of pure xenon atoms was introduced into the chamber by expansion through a 50 μm nozzle with a backing pressure of 1 bar. This leads to a pressure of 3×10^{-4} mbar in the expansion chamber. The central part of the supersonic expansion was selected by a 1.0 mm conically shaped skimmer allowing us to

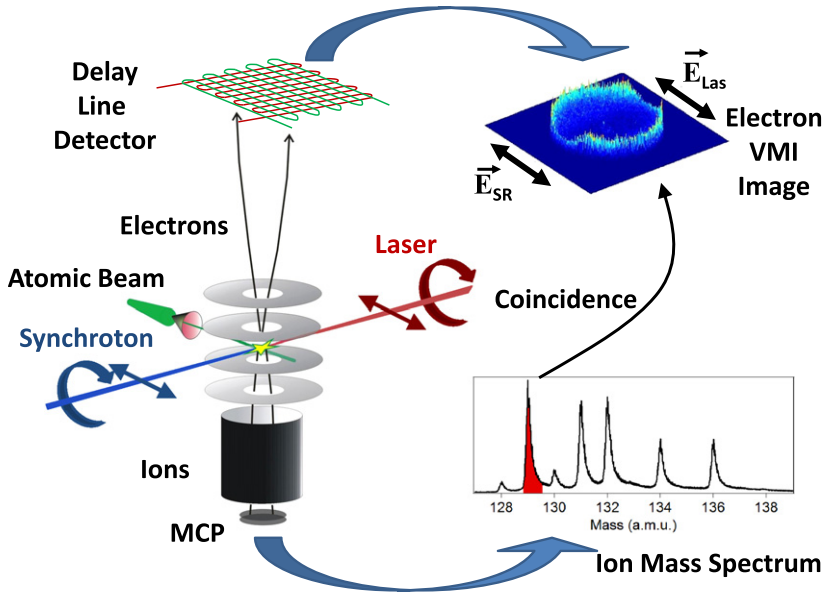

Figure 1. The schematic layout of the experimental set-up. This figure depicts the electrostatic optics used to guide the electrons into a velocity map imaging spectrometer while simultaneously sending the ions into a time-of-flight spectrometer terminated by a multichannel plate detector. The electrons and ions are produced by the interaction of the synchrotron light from the DESIRS beam line at the French synchrotron SOLEIL, a continuous wave optical laser and a skimmed beam of Xe atoms. The arrows illustrate the variable polarization of the counter-propagating synchrotron and laser beams. The signals taken from both detectors are amplified, discriminated and recorded by a time to digital converter (TDC) and computer. This allows the velocity map image produced in coincidence with each ion mass to be extracted from the data.

reduce the background pressure in the interaction chamber to 2×10^{-7} mbar while reducing the volume of the interaction region. The atomic beam then crossed the counter propagating synchrotron radiation (SR) and laser photon beams at right angles at the center of the ionization chamber.

The quasi-continuous VUV (10.401 eV) photons for excitation to the intermediate 5d $[\frac{3}{2}]_1$ resonance were delivered by the DESIRS beamline via the OPHELIE2 variable polarization undulator [15]. After traversing a gas filter [16] filled with Ar to remove higher order harmonics, the photons are then dispersed with a 2400 gr mm^{-1} SiC grating. The entrance and exit slits were set to provide a resolution of 0.16 meV and a photon flux of $\approx 5 \times 10^{10}$ photons s^{-1}. The beam size at the sample level is estimated at 200 mm $\times$ 80 mm for the direction perpendicular and parallel to the detector axis, respectively. The Stokes parameters are measured at the sample level via a three-reflexion polarimeter [17] so that the polarization state of the photons is controlled and precisely known over the whole energy range of the beamline. The measured degrees of linear and circular polarization reach values of $\geqslant$0.99 and $\geqslant$0.97, respectively.

The excited atoms were subsequently excited to the autoionizing 4f' $[\frac{5}{2}]_2$ state by a conventional continuous wave linear dye laser pumped by the 532 nm light of a frequency-doubled solid state laser (5W VERDI). Using a rhodamine 6G dye an average laser power of 800 mW and a spectral width of about 1.3 cm^{-1} was obtained in the maximum of the emission curve of the dye (595 nm). Changing the wavelength in the range from 569.1 to 571.2 nm allowed us to scan across the Fano profile of the 5d $[\frac{3}{2}]_1 \longrightarrow$ 4f' $[\frac{5}{2}]_2$ resonance. The polarization states of both the SR and the visible laser light could be changed between linear horizontal (perpendicular to the direction of the principal axis of the spectrometer) and left and right circular polarization. The polarization of the SR is controlled by a variable polarization undulator from the beamline control system while that of the laser light is changed either by insertion of a half or a quarter waveplate.

The ions and electrons resulting from the ionization process were accelerated in opposite directions perpendicular to the molecular and photon beams inside the DELICIOUS II angle-resolving photoelectron-photoion coincidence imaging spectrometer [18] which consists of an electron velocity mapping imaging (VMI) spectrometer and a linear Wiley McLaren-type ion time of flight (TOF) spectrometer. The spectrometer was operated in the coincidence mode so that each electron could be tagged according to the flight time (and consequently mass) of the ion formed in the same event. In this mode the acquisition system is triggered by the arrival of the electron on the MCP of the VMI delay line detector. This opens a window for the time to digital converter (model CTNM4, Institut de Physique Nucléaire, Orsay, France) to accept the four signals from the delay line detector [19] and the ion signal from the TOF spectrometer. All of the events are stored and are sorted later by the software to extract all of the information either in single hit or in coincidence. In a typical TOF spectrum the various natural isotopes of Xe can be easily separated by the apparatus (see the inset of figure 1 for

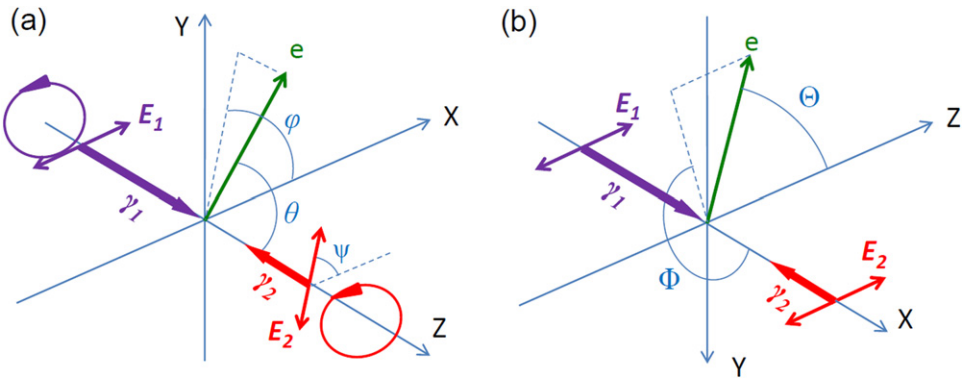

Figure 2. Coordinate systems: (a) general for circularly and linearly polarized light beams; (b) for linearly polarized beams with parallel polarizations. γ_1 and γ_2 correspond to XUV and optical photons, respectively.

an example of the TOF spectrum). By selecting a range of arrival times and thus masses of the ions we can select only the electrons formed in coincidence with ions of that mass and therefore a velocity mapped photoelectron image for each isotope can be built up. These images were then inverted using the pBasex software [20] in order to extract the parameters describing the electron angular distributions resulting from ionization of the $I = 0(^{132,134,136}\mathrm{Xe})$, $I = \frac{1}{2}$ (^{129}Xe) and $I = \frac{3}{2}$ (^{131}Xe) atoms.

3. Theoretical description of the two-photon ionization

The general theoretical approach to treat the two-photon ionization process is based on the formalism of statistical tensors [21] applied to the PADs in photoionization of polarized atoms [22]. We describe the interaction of the electromagnetic field with the atom in the dipole approximation.

3.1. Polarization of the intermediate atomic state

The electronic shell of the intermediate atomic state with total angular momentum J_0 after absorption of the photon by the initially unpolarized atom assumes the polarization distribution described by the set of statistical tensors

$$\rho_{k_0q_0}(J_0) = \delta_{k_0k_1}\delta_{q_0q_1}3(-1)^{J_0+J_i+k_1+1}\begin{Bmatrix}1 & J_0 & J_i\\ J_0 & 1 & k_1\end{Bmatrix}\rho^{\gamma_1}_{k_1q_1}. \tag{3}$$

Here J_i is the angular momentum of the electronic shell in the initial atomic state, the standard notation for the Wigner 6j-coefficient is used, and the statistical tensors $\rho^{\gamma_1}_{k_1q_1}$ ($0 \leqslant k_1 \leqslant 2$, $-k_1 \leqslant q_1 \leqslant k_1$) describe the polarization of the photon $\hbar\omega_1$. Thus the polarization of the excited atom is characterized only by those statistical tensors (3) that are present in the description of the photon beam if not being cut by the triangle rule $k_0 \leqslant \min\{2J_0, 2\}$.

We choose the z axis of the laboratory system to coincide with the axis of the collinear radiation beams (figure 2(a)). Then the nonvanishing photon statistical tensors are expressed in terms of the Stokes parameters of the radiation p_1, p_2, p_3 as [21]: $\rho^{\gamma}_{00} = \frac{1}{\sqrt{3}}$; $\rho^{\gamma}_{10} = \frac{1}{\sqrt{2}}p_3$; $\rho^{\gamma}_{20} = \frac{1}{\sqrt{6}}$; $\rho^{\gamma}_{2\pm2} = -\frac{1}{2}p_\ell \exp[\mp 2i\phi]$, where $p_\ell = \sqrt{p_1^2 + p_2^2}$, $\cos 2\phi = \frac{p_1}{p_\ell}$ and $\sin 2\phi = \frac{p_2}{p_\ell}$. The angle ϕ (not shown in figure 2(a)) indicates the principal axis of the polarization ellipse with respect to the fixed x axis. The Stokes parameters $p_1 = +1(-1)$ and $p_2 = +1(-1)$ describe radiation which is completely linearly polarized in the direction $\varphi = 0$ ($\varphi = \frac{\pi}{2}$) and $\varphi = \frac{\pi}{4}$ ($\varphi = \frac{3\pi}{4}$), respectively. The Stokes parameter $p_3 = +1(-1)$ corresponds for the circularly polarized light to the positive (negative) value of the photon helicity.

The statistical tensors of the electronic shell (3) evolve in the time interval between the absorption of the first and the second photon. With respect to the present experimental conditions, there is one dominating effect that has to be taken into account, namely the hyperfine interactions causing precession of the angular momentum of the electronic shell around the total atomic angular momentum. Each tensor (3) then gains a depolarization factor $h_k(I)$ accounting for this precession: $\rho_{k_0q_0}(J_0) \to h_{k_0}(I)\rho_{k_0q_0}(J_0)$.

The theory of depolarization [4, 5] implies that the nuclear spin is uncoupled from the electronic shell during the photoexcitation. Taking also into account that in our experiment the atoms are exposed to long radiation pulses and the instant of excitation during the pulse is undefined, the depolarization factors are

expressed as [5]

$$h_k(I) = \frac{1}{\hat{I}^2}\sum_{FF'}\hat{F}^2\hat{F}'^2\begin{Bmatrix} F & F' & k \\ J_0 & J_0 & I \end{Bmatrix}^2\left(1+\frac{\omega_{FF'}^2}{\Gamma^2}\right)^{-1}, \tag{4}$$

where the sum is taken over the hyperfine structure (HFS) levels of the electronic state with angular momentum J_0, Γ is the natural width, which we assume identical for all the hyperfine levels; we use abbreviation $\hat{a} \equiv \sqrt{2a+1}$ and denote $\omega_{FF'} = (E_F - E_{F'})/\hbar$, where E_F is the energy of a hyperfine level. The identity $h_0(I) = 1$ follows from (4) and corresponds to the fact that the zero rank tensor, i.e. the population of the excited state, is unaffected by the precession. For completely overlapping HFS ($\omega_{FF'} = 0$), again, the depolarization does not occur ($h_k(I) = 1$). On the contrary, well separated HFS ($\omega_{FF'} \gg \Gamma$ for $F \neq F'$) are described by the lowest possible values of $h_k(I)$ and maximal depolarization.

3.2. Photoelectron angular distribution

The PAD for the isotope with nuclear spin I can be cast into the form [22]

$$\left(\frac{\mathrm{d}\sigma}{\mathrm{d}\Omega}\right)_I = \pi\alpha\omega\sum_{\substack{k_1q_1k_2q_2\\kq}} B_{k_1kk_2}\,\rho_{k_2q_2}^{\gamma_2}\,h_{k_1}(I)\rho_{k_1q_1}\left(J_0\right)\left(k_1q_1,\,k_2q_2\,\middle|\,kq\right)\frac{1}{\sqrt{4\pi}\hat{k}}Y_{kq}(\vartheta,\,\varphi), \tag{5}$$

where $\rho_{k_2q_2}^{\gamma_2}$ are the statistical tensors of the second photon $\hbar\omega_2$, $Y_{kq}(\vartheta,\,\varphi)$ is the spherical harmonic in the Condon–Shortley phase convention, and $\left(j_1m_1,\,j_2m_2\,|\,jm\right)$ is the Clebsch–Gordan coefficient. The parameters

$$B_{k_1kk_2} = \hat{k}_1\hat{k}_2\sum_{\substack{ll'jj'\\JJ'}}(-1)^{J_f+J+k-1/2}\hat{l}\hat{l}'\hat{j}\hat{j}'\hat{J}\hat{J}'\,(l0,\,l'0\,|\,k0)\begin{Bmatrix} j & l & \frac{1}{2} \\ l' & j' & k \end{Bmatrix}\begin{Bmatrix} J_0 & 1 & J \\ J_0 & 1 & J' \\ k_1 & k_2 & k \end{Bmatrix}D_{ljJ}D^*_{l'j'J'} \tag{6}$$

contain information about the dynamics of photoionization. Here J is the total electronic angular momentum of the system 'ion + photoelectron' and the standard notation for 9j-coefficients are used. The reduced dipole matrix elements D_{ljJ} describe ionization into the channel with the quantum numbers l, j, J. The dynamical parameters (6) satisfy the relation $B_{k_1kk_2} = (-1)^{k_1+k_2+k}B^*_{k_1kk_2}$, i.e. they are either real or imaginary. The indices k_1 and k_2 take the values 0, 1 and 2 and are subject to the triangle rule $|k_1 - k_2| \leqslant k \leqslant k_1 + k_2$. Due to the conservation of parity k takes only even values.

Note that the dynamics of the electron transitions (the matrix elements) does not depend on the nuclear spin; in our treatment the latter affects the PAD only via the depolarization factors $h_k(I)$ in equation (5).

Interference between amplitudes of direct photoionization and photoionization via excitation of an isolated autoionizing state is taken into account according to [22, 23]. For an autoionizing state described by the total electronic angular momentum J_r (in our example $J_r = 2$) and decay into a single state of the residual ion, the reduced matrix elements of the dipole operator are expressed in the form

$$D_{ljJ} = \mathrm{e}^{\mathrm{i}\Delta_{ljJ}}\left(\delta_{JJ_r}\sum_{l'j'}d_{l'j'J_r}\frac{V_{ljJ_r}V^*_{l'j'J_r}}{\sum_{l''j''}\left|V_{l''j''J_r}\right|^2}\,\frac{q-\mathrm{i}}{\varepsilon+\mathrm{i}} + d_{ljJ}\right). \tag{7}$$

Here $d_{ljJ} = \langle ljJ \,||\, D \,||\, J_0\rangle$ is the matrix element of the direct transition to the continuum channel with quantum numbers l, j, and J, Δ_{ljJ} is the phase shift in this channel, $V_{lj} = \langle ljJ_r \,||\, V \,||\, J_r\rangle$ is the matrix element coupling the discrete (autoionizing) state with the continuum, q is the Fano profile index in photoabsorption, $\varepsilon = 2(E - E_r)/\Gamma_r$ is the relative energy and E_r is the resonance position. The total width of the autoionizing resonance is given as $\Gamma_r = 2\pi\sum_{lj}|V_{ljJ_r}|^2$. The profile index and the width in (7) are considered as constants in the region of the resonance.

In the rest of the manuscript we specify equations for the intermediate state with $J_0 = 1$ photoexcited from the state with $J_i = 0$.

3.3. Circularly polarized radiation beams

The geometry with two circularly polarized counter-propagating light beams is shown in figure 2(a). The PAD can be described in terms of two asymmetry parameters in the following manner:

$$\left(\frac{\mathrm{d}\sigma}{\mathrm{d}\Omega}\right)_I^{+\pm} = \frac{\sigma_I^{+\pm}}{4\pi}\left(1 + \beta_2^{+\pm}(I)\,\mathrm{P}_2(\cos\theta) + \beta_4^{+\pm}(I)\,\mathrm{P}_4(\cos\theta)\right), \tag{8}$$

where

$$\beta_2^{+\pm}(I) = \frac{2\mathcal{B}_{022} + h_2(I)\left(2\mathcal{B}_{220} - \mathcal{B}_{222}\right) \pm h_1(I)\mathcal{B}_{121}}{\mathcal{B}_{000} \mp h_1(I)\mathcal{B}_{101} + h_2(I)\mathcal{B}_{202}}, \tag{9}$$

$$\beta_4^{+\pm}(I) = \frac{48h_2(I)\mathcal{B}_{242}}{\mathcal{B}_{000} \mp h_1(I)\mathcal{B}_{101} + h_2(I)\mathcal{B}_{202}}. \tag{10}$$

Here and below we introduce shortened notations for the real parameters $\mathcal{B}_{000} = \frac{1}{3}B_{000}$, $\mathcal{B}_{202} = \frac{\sqrt{5}}{6}B_{202}$, $\mathcal{B}_{022} = \frac{\sqrt{10}}{12}B_{022}$, $\mathcal{B}_{220} = \frac{\sqrt{10}}{12}B_{220}$, $\mathcal{B}_{222} = \frac{5\sqrt{14}}{42}B_{222}$, $\mathcal{B}_{242} = \frac{\sqrt{70}}{672}B_{242}$, $\mathcal{B}_{122} = \frac{\sqrt{30}}{12}\Im B_{122}$, $\mathcal{B}_{101} = \frac{\sqrt{3}}{2}B_{101}$, $\mathcal{B}_{121} = \frac{\sqrt{6}}{2}B_{121}$ and we will omit the argument I, when it does not lead to a confusion. The superscripts in (8)–(10) indicate the polarization states of the photons: ++ and +− for the parallel and antiparallel spins of the circularly polarized photons (we use the convention that the first sign corresponds to the SR and '+' is assigned to the direction of the z axis).

The angle integrated cross section obtained from equations (5), (6) is given by

$$\sigma_I^{+\pm} = \pi\alpha\omega\left[\left(1 \pm \frac{3}{4}h_1 + \frac{1}{20}h_2\right)\sum_{lj}\left|D_{ljJ=2}\right|^2 + \left(1 \mp \frac{3}{4}h_1 - \frac{1}{4}h_2\right)\sum_{lj}\left|D_{ljJ=1}\right|^2 + \left(1 \mp \frac{3}{2}h_1 + \frac{1}{2}h_2\right)\sum_{lj}\left|D_{ljJ=0}\right|^2\right]. \tag{11}$$

This leads to the integral CD in the form

$$\mathrm{CD} \equiv \frac{\sigma^{++} - \sigma^{+-}}{\sigma^{++} + \sigma^{+-}} = \frac{\frac{3}{4}h_1\sum_{lj}\left(\left|D_{ljJ=2}\right|^2 + \left|D_{ljJ=1}\right|^2 + 2\left|D_{ljJ=0}\right|^2\right)}{\sum_{lj}\left[\left(1 + \frac{1}{20}h_2\right)\left|D_{ljJ=2}\right|^2 + \left(1 - \frac{1}{4}h_2\right)\left|D_{ljJ=1}\right|^2 + \left(1 + \frac{1}{2}h_2\right)\left|D_{ljJ=0}\right|^2\right]}. \tag{12}$$

Neglecting depolarization ($h_k = 1$), for circularly polarized radiation beams with parallel spins, it follows immediately from equation (11) that only channels with $J = 2$ contribute to the cross section σ_I^{++}. This result is obvious from the selection rules for the projection of the total electronic angular momentum, which for this case can only take the maximal absolute value of two. By the same reasoning the asymmetry parameters (9) and (10) contain contributions only from the channels with $J = 2$. In our formalism this follows from the properties of the 9j symbol in equation (6). For parallel photon spins, the contributions from channels with $J = 0$ and $J = 1$ have to be taken into account when depolarization occurs, since other magnetic substates can be populated in the intermediate excited state.

3.4. Linearly polarized radiation beams

When both the SR and laser fields are linearly polarized, the PAD depends on the adjustable angle ψ between the polarization directions of the photon beams (figure 2(a)). Choosing the x axis of the laboratory system along the electric field of the SR and substituting the corresponding statistical tensors of the photons into equation (5), the PAD can be cast into the form

$$\begin{aligned}\left(\frac{\mathrm{d}\sigma}{\mathrm{d}\Omega}\right)_I = \frac{\pi\alpha\omega}{4\pi}\Big(&\mathcal{B}_{000} + h_2\mathcal{B}_{202}(1 + 3\cos 2\psi) \\ &+ \mathcal{B}_{022}\left[2P_2(\cos\vartheta) - \cos(2\varphi - 2\psi)P_2^2(\cos\vartheta)\right] \\ &+ h_2\mathcal{B}_{220}\left[2P_2(\cos\vartheta) - \cos 2\varphi\, P_2^2(\cos\vartheta)\right] \\ &+ h_2\mathcal{B}_{222}\left[(3\cos 2\psi - 1)P_2(\cos\vartheta) - P_2^2(\cos\vartheta)\cos(2\varphi - \psi)\cos\psi\right] \\ &+ h_2\mathcal{B}_{242}\Big[24(2 + \cos 2\psi)P_4(\cos\vartheta) - 8P_4^2(\cos\vartheta)\cos(2\varphi - \psi)\cos\psi \\ &+ P_4^4(\cos\vartheta)\cos(4\varphi - 2\psi)\Big]\Big).\end{aligned} \tag{13}$$

The angle-integrated ionization cross section can be obtained by integration of (13) over the angles of the photoemission:

$$\sigma_I^{\rm lin} = \pi\alpha\omega\Bigg[\left(1+\frac{1}{20}h_2(1+3\cos 2\psi)\right)\sum_{lj}\left|D_{ljJ=2}\right|^2 + \left(1-\frac{1}{4}h_2(1+3\cos 2\psi)\right)\sum_{lj}\left|D_{ljJ=1}\right|^2 + \left(1+\frac{1}{2}h_2(1+3\cos 2\psi)\right)\sum_{lj}\left|D_{ljJ=0}\right|^2\Bigg], \tag{14}$$

where the superscript 'lin' indicates two linearly polarized light beams.

The integral LD is defined as the normalized difference between the cross sections (14) for parallel ($\psi = 0$) and perpendicular ($\psi = \frac{\pi}{2}$) polarizations of the radiation beams:

$$\mathrm{LD} \equiv \frac{\sigma^{\parallel}-\sigma^{\perp}}{\sigma^{\parallel}+\sigma^{\perp}} = \frac{\frac{3}{4}h_2\left(\frac{1}{5}\left|D_{J_i,jJ=2}\right|^2 - \left|D_{J_i,jJ=1}\right|^2 + 2\left|D_{J_i,jJ=0}\right|^2\right)}{\left(1+\frac{1}{20}h_2\right)\left|D_{J_i,jJ=2}\right|^2 + \left(1-\frac{1}{4}h_2\right)\left|D_{J_i,jJ=1}\right|^2 + \left(1+\frac{1}{2}h_2\right)\left|D_{J_i,jJ=0}\right|^2}. \tag{15}$$

For $\psi = 0$ and neglecting depolarization of the intermediate state ($h_2 = 1$), channels with $J = 1$ do not contribute into the integral cross section (14). Under these conditions the channel $J = 1$ also does not contribute to the differential cross section (13).

In correspondence with the geometry used in the experiment, we concentrate on the case when the fields are polarized in the same direction ($\psi = 0$). Then in the coordinate system with the z-axis chosen along the polarization (figure 2(b)), equation (13) (after substitution $\cos\Theta = \sin\vartheta\cos\varphi$, $\cot\Phi = -\cot\vartheta/\sin\varphi$) acquires a simple form :

$$\left(\frac{\mathrm{d}\sigma}{\mathrm{d}\Omega}\right)_I = \frac{\sigma_I^{\rm lin}}{4\pi}\Big(1+\beta_2^{\rm lin}P_2(\cos\Theta)+\beta_4^{\rm lin}P_4(\cos\Theta)\Big), \tag{16}$$

where $\beta_2^{\rm lin}$ and $\beta_4^{\rm lin}$ are the asymmetry parameters:

$$\beta_2^{\rm lin} = -4\frac{h_2\left(\mathcal{B}_{220}+\mathcal{B}_{222}\right)+\mathcal{B}_{022}}{\mathcal{B}_{000}+4h_2\mathcal{B}_{202}}, \tag{17}$$

$$\beta_4^{\rm lin} = \frac{192h_2\mathcal{B}_{242}}{\mathcal{B}_{000}+4h_2\mathcal{B}_{202}}. \tag{18}$$

3.5. Case of dominating $J = 2$ channels

Since the autoionizing state with $J_r = 2$ interacts only with $J = 2$ ionization channels, we will call the $J = 2$ channels the 'resonance' channels. Note that the resonance channels $J = 2$ are reached also via direct photoionization by the second photon. It is instructive to consider the case of dominating resonance channels. Then the expressions for the PAD and the dichroism are considerably simplified due to neglecting terms with $J = 0,\ 1$ and due to additional relationships between the parameters $\mathcal{B}_{k_1kk_2}$: $20\mathcal{B}_{202} = -\frac{4}{3}\mathcal{B}_{101} = \mathcal{B}_{000}$, $\mathcal{B}_{220} = 6\mathcal{B}_{121} = -\frac{7}{2}\mathcal{B}_{222} = \mathcal{B}_{022}$ and $\mathcal{B}_{221} = \mathcal{B}_{122} = 0$. As a result, equations (9), (10) can be simplified to:

$$\beta_2^{+\pm} = \frac{2+\frac{16}{7}h_2 \pm 6h_1}{1\pm\frac{3}{4}h_1+\frac{1}{20}h_2}\cdot\frac{\mathcal{B}_{022}}{\mathcal{B}_{000}}, \tag{19}$$

$$\beta_4^{+\pm} = \frac{48h_2}{1\pm\frac{3}{4}h_1+\frac{1}{20}h_2}\cdot\frac{\mathcal{B}_{242}}{\mathcal{B}_{000}}. \tag{20}$$

The asymmetry parameters (17) and (18) take the form

$$\beta_2^{\rm lin} = -\frac{20}{7}\frac{7+5h_2}{5+h_2}\cdot\frac{\mathcal{B}_{022}}{\mathcal{B}_{000}} \quad \beta_4^{\rm lin} = \frac{960h_2}{5+h_2}\cdot\frac{\mathcal{B}_{242}}{\mathcal{B}_{000}}. \tag{21}$$

The CD (12) and the LD (15) depend only on the depolarization factors:

$$\mathrm{CD} = \frac{15h_1}{20 + h_2}, \qquad \mathrm{LD} = \frac{3h_2}{20 + h_2}. \tag{22}$$

For the case of the perfectly polarized intermediate discrete state ($h_k = 1$) keeping only $J = 2$ channels one has the relations:

$$\beta_2^{\mathrm{lin}} = \beta_2^{(+-)} = -\beta_2^{(++)}, \qquad \beta_4^{\mathrm{lin}} = \beta_4^{(+-)} = 6\beta_4^{(++)}, \tag{23}$$

and

$$\mathrm{CD} = 5\ \mathrm{LD}. \tag{24}$$

From the last equality it is expected that the CD is much larger than the LD.

3.6. Atomic model

The atomic model used in the numerical calculations of the matrix elements is the same as presented in [13]. Here we outline it in more detail. Atomic wave functions were obtained within an intermediate-coupling multiconfiguration Hartree–Fock (MCHF) approximation [24] with the basis term-average electron orbitals generated with the frozen $Xe^+\ 5p^5$ core. We accounted for the $5p^5$(6–9)s, (5–7)d configurations for the intermediate discrete state with the leading terms

$$5p^5(^2P_{3/2})5d[3/2]_1 = 0.779\left(5p^5\ 5d\ ^1P\right) - 0.624\left(5p^5\ 5d\ ^3D\right) - 0.050\left(5p^5\ 6s\ ^1P\right) - 0.023\left(5p^5\ 6s\ ^3P\right) + ... \tag{25}$$

For the autoionizing state the configurations $5p^5$4f, 5f, 6p were included leading to the wave function

$$5p^5(^2P_{1/2})4f[5/2]_2 = 0.573\left(5p^5\ 4f\ ^1D\right) - 0.467\left(5p^5\ 4f\ ^3D\right) + 0.673\left(5p^5\ 4f\ ^3F\right) + ... \tag{26}$$

Note that the intermediate-coupling mixing coefficients in (26) are very close to those of the pure jK coupling scheme, where the corresponding expansion coefficients are $2/3 \approx 0.667$, $1/\sqrt{3} \approx 0.577$ and $-\sqrt{2}/3 \approx -0.471$. On the one hand, in the pure jK coupling scheme in single configuration approximation the autoionization $5p^5(^2P_{1/2})4f[5/2]_2 \rightarrow 5p^5\ ^2P_{3/2} + Ef$ via the Coulomb interaction is strictly forbidden, provided the common set of electron orbitals is used in the wave functions of the autoionizing and the final ionic states. On the other hand, the overlap between radial components of the 4f and *Ef* electron wave functions, governing the decay amplitude, is much larger than that between 4f and *Ep* functions. Therefore, the decay into the dominating *Ef* channel proceeds in our model due to a tiny violation of the pure jK-coupling scheme for the $4f'[\frac{5}{2}]_2$ state. Furthermore strong mutual cancellation takes place in the matrix element of the dipole transition between the discrete $5d[\frac{3}{2}]_1$ and the autoionizing $4f'[\frac{5}{2}]_2$ states. As a result, although contributions of higher configurations into the wave functions of the autoionizing and excited discrete state are small, they are extremely important for the correct calculation of the autoionizing width and the profile of the resonance [13]. The high sensitivity of the resonance parameters to the details of the atomic model has been outlined in [25]. For example, our full model gives the natural width of the $4f'[\frac{5}{2}]_2$ state $\Gamma_r = 0.35$ meV, with the single-configuration result $\Gamma_r = 0.46$ meV. These values can be compared to the measured width $\Gamma_r = 0.41 \pm 0.04$ meV from [26] and $\Gamma_r = 0.36 \pm 0.05$ meV from [27] as well as with $\Gamma_r = 0.50$ and $\Gamma_r = 0.42$ meV obtained in configuration interaction Pauli–Fock approach including core polarization in [25] and [28], respectively.

4. Results and discussion

4.1. Isotope effects on the dichroism

Table 1 presents experimental and theoretical results for LD and CD measured for different isotopes. The values of the LD are much smaller than the values of the CD, as has been expected considering the discussion in section 3.5.

For the LD, the calculated values are in agreement with the experimental values within the experimental error bars. Since the CD values are much larger, the comparison between experiment and theory is more meaningful. The agreement between experiment and theory for the $I = 0$ isotopes is very good. Thus, the CD data for the $I = 0$ isotopes confirm the negligible effect of depolarization of the Xe^* atoms in the reaction volume due to reasons other than the hyperfine interaction [13]. The values of the dichroism for the isotopes with $I = \frac{1}{2}$ and $I = \frac{3}{2}$ are smaller than for the isotopes with $I = 0$. This is clear evidence for the depolarization of the intermediate electronic state due to hyperfine interactions. For the ^{129}Xe ($I = \frac{1}{2}$) isotope the measured CD and the CD calculated for separated HFS levels are again in excellent agreement. This confirms that for this isotope the HFS

Table 1. Linear and circular dichroism. Second column: experimental values for the dichroism at the resonance energy E_r of the laser photon; third column: theoretical values obtained with taking into account only the resonance $J = 2$ channels in the limit of separated HFS levels according to equations (22); fourth column: same as third column, but with including the 'weak' ionization channels with $J = 0,1$ according to equations (12) and (15) (at the resonance energy E_r).

Nuclear spin	Exp	Theory $J=2$	Theory $J = 0, 1, 2$
	LD		
$I=0$	0.11(2)	$\frac{1}{7} \approx 0.144$	0.14
$I=\frac{1}{2}$	0.03(3)	$\frac{3}{61} \approx 0.049$	0.049
$I=\frac{3}{2}$	0.04(3)	$\frac{111}{3037} \approx 0.037$	0.037
	CD		
$I=0$	0.67(2)	$\frac{5}{7} \approx 0.714$	0.71[a]
$I=\frac{1}{2}$	0.54(4)	$\frac{35}{61} \approx 0.574$	0.57
$I=\frac{3}{2}$	0.43(3)	$\frac{950}{3037} \approx 0.313$	0.31

[a] The value CD = 0.68 in [13] was given for the integral over the profile of the resonance.

levels are well separated and the depolarization is maximal. In contrast, there is a noticeable disagreement between the calculated CD for the ^{131}Xe ($I = \frac{3}{2}$) isotope in the limiting case of separated HFS levels and experiment. Thus, the measured CD may be used to draw some conclusions on the hyperfine interactions in the ^{131}Xe $5d[\frac{3}{2}]_1$ state.

To proceed further we account for the dominating magnetic interaction term in the expression for the energy difference between the HFS levels, $\omega_{FF'} = A\ F$, where A is a HFS coupling constant for the Xe $5d[\frac{3}{2}]_1$ state and $F' = F - 1$. Thus the hyperfine splitting for a fixed isotope depends only on the single parameter A. Substituting the above expression for $\omega_{FF'}$ into equation (4), one obtains

$$h_1(1/2) = \frac{7}{9} + \frac{2}{9} \cdot \frac{1}{1 + \frac{9}{4}\alpha} \rightarrow \frac{7}{9} \approx 0.78, \tag{27}$$

$$h_2(1/2) = \frac{1}{3} + \frac{2}{3} \cdot \frac{1}{1 + \frac{9}{4}\alpha} \rightarrow \frac{1}{3} \approx 0.33, \tag{28}$$

$$h_1(3/2) = \frac{19}{45} + \frac{5}{18} \cdot \frac{1}{1 + \frac{9}{4}\alpha} + \frac{3}{10} \cdot \frac{1}{1 + \frac{25}{4}\alpha} \rightarrow \frac{19}{45} \approx 0.42, \tag{29}$$

$$h_2(3/2) = \frac{37}{150} + \frac{1}{30} \cdot \frac{1}{1 + \frac{9}{4}\alpha} + \frac{3}{10} \cdot \frac{1}{1 + 16\alpha} + \frac{21}{50} \cdot \frac{1}{1 + \frac{25}{4}\alpha} \rightarrow \frac{37}{150} \approx 0.25, \tag{30}$$

where $\alpha = (A/\Gamma)^2$. Note that the values of α are different for isotopes with $I = \frac{1}{2}$ (equations (27) and (28)) and $I = \frac{3}{2}$ (equations (29) and (30)). The limits indicated at the right sides of equations (27)–(30) are reached when the HFS levels are well separated ($\alpha \gg 1$). In this limit, the depolarization factors for the $I = \frac{1}{2}$ isotope are closer to unity than the depolarization factors for the $I = \frac{3}{2}$ isotope, which is in accordance with an intuitive expectation of larger depolarization for an isotope with larger nuclear spin.

Substituting (29) and (30) into (22) we find from the value of the CD, $\alpha = 0.71 \pm 0.21$, estimate $|A|/\Gamma = 0.85 \pm 0.14$, and the depolarization factors $h_1(3/2) = 0.58 \pm 0.04$, $h_2(3/2) = 0.35 \pm 0.04$. The latter numbers are essentially larger than 0.42 and 0.25, respectively, in the limit of the separated HFS levels (see (29) and (30)) and are much closer to the depolarization factors for the ^{129}Xe isotope with $I = \frac{1}{2}$. Thus the HFS splitting of the ^{131}Xe $5d[\frac{3}{2}]_1$ appears to be smaller than the natural width.

Information on the HFS of the $5p^5 5d$ configuration in the Xe atom is rather scarce. To our knowledge the HFS coupling constant A has neither been measured nor calculated for the $5d[\frac{3}{2}]_1$ state, although in a few studies the HFS of the 5d states in Xe have been discussed, for example [29–35]. According to the isotopic scaling of the A values, the coupling constants should scale between ^{129}Xe and ^{131}Xe as the ratio of their nuclear magnetic

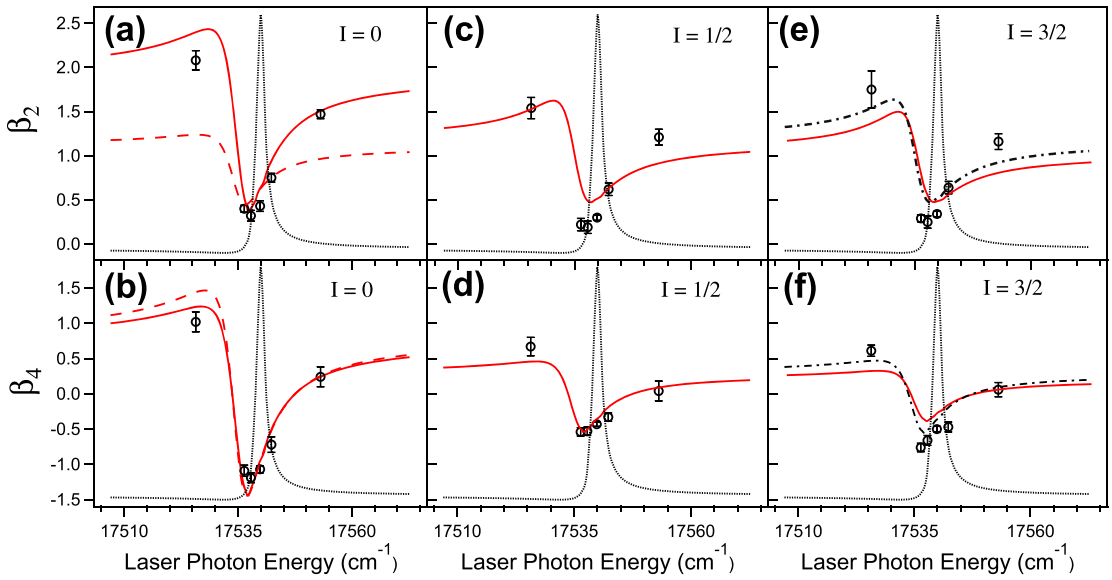

Figure 3. $\beta_2^{\rm lin}$ (top) and $\beta_4^{\rm lin}$ (bottom) parameters for Xe ions with nuclear spin $I = 0$ (panels (a) and (b)), $I = \frac{1}{2}$ (panels (c) and (d)) and $I = \frac{3}{2}$ (panels (e) and (f)) at different laser wavelengths across the $5d[\frac{3}{2}]_1 + \gamma_{las} \rightarrow 4f'[\frac{5}{2}]_2$ resonance. The experimental data (open circles) are extracted from the VMI images recorded in coincidence. The MCHF results (solid) are obtained assuming well isolated hyperfine structure states ($\alpha \gg 1$) for the isotopes with nonzero spin (panels (c)–(f)). Chain curves in the panels (e) and (f) present results for the $I = \frac{3}{2}$ isotope with α obtained in this work. The dashed curves in panels (a) and (b) show results with accounting only for resonant channels with $J = 2$. The profile of the $4f'[\frac{5}{2}]_2$ resonance in the angle-integrated cross section σ is shown for comparison (dotted line).

moments ($\mu_{129} = -0.7768\mu_N$, $\mu_{131} = +0.6908\mu_N$, where μ_N is the nuclear magneton) times the reciprocal of their respective nuclear spin, resulting in the factor $A(^{131}\text{Xe})/A(^{129}\text{Xe}) = -0.296$. Thus, the HFS splitting for the ^{129}Xe isotope is expected to be more than three times larger than for the ^{131}Xe isotope and the parameter α for ^{129}Xe should be around 8, which does not contradict the conclusion about well separated HFS levels ($\alpha \gg 1$), found above for the ^{129}Xe $5d[\frac{3}{2}]_1$ state.

The lifetime (natural width Γ) of the Xe $5d[\frac{3}{2}]_1$ state has never been directly measured. To estimate the absolute value of A for the ^{131}Xe $5d[\frac{3}{2}]_1$ state, we make a reliable assumption that Γ is determined by radiative transition to the ground state of Xe and take a well established experimental value for the oscillator strength of this transition [36]. Then we obtain $\Gamma \approx 95$ MHz and estimate $|A| \approx 80$ MHz (or 2.7 mK). This value is a few times less than most of the available coupling constants A for the 5d manifold (scaled to the ^{131}Xe isotope) [29, 33], comparable to $A = 138 \pm 1$ MHz measured for the $5d[\frac{5}{2}]_3$ state in ^{131}Xe [34] and larger than predicted for the $5d[\frac{3}{2}]_2$ state [29].

4.2. Isotope effects in PADs

Figure 3 presents the asymmetry parameters (17) and (18) in the region around the $5p^5(^2P_{1/2})4f[5/2]_2$ resonance for isotopes with different nuclear spins. The parameter $\beta_4^{\rm lin}$ would vanish for an unpolarized intermediate $5p^5(^2P_{3/2})5d[3/2]_1$ state. The high values reached by $\beta_4^{\rm lin}$ indicate large anisotropy (alignment) of this state. In a previous publication [13] we concentrated on the PADs measured in coincidence with the $I = 0$ ions. For completeness of the present discussion part of this data is included in panels (a) and (b) of figure 3. From panels (a) and (b) it can be seen that if only the resonant channels with $J = 2$ are included in the calculation of the asymmetry parameters according to (21) (with $h_1 = h_2 = 1$), the theoretical model does not reproduce the experimental values. Only when the 'weak' channels ($J = 0, 1$) are included we can achieve satisfactory agreement. The calculation of the atomic structure does not differ for different isotopes, and since the model gives good agreement with experiment for $I = 0$, it is obligatory that it be also used for the $I = \frac{1}{2}$ and $I = \frac{3}{2}$ isotopes. However, it is incorrect to think that the results for the asymmetry parameters for the latter isotopes should be automatically as good as for the $I = 0$ isotopes, once the depolarization due to the coupling between the electronic and nuclear angular momenta is properly included. Indeed, the depolarization of the intermediate state for the cases $I = \frac{1}{2}$ and $I = \frac{3}{2}$ leads to the opening of ionization channels with $J = 1$, while the quality of our approximations for the $J = 1$ channels is not verified by the process with the $I = 0$ isotopes, where these channels

Table 2. Measured and calculated asymmetry parameters for linearly polarized fields at resonant energy E_r.

	Experiment			Theory		
Isotope	$I=0$	$I=\frac{1}{2}$	$I=\frac{3}{2}$	$I=0$	$I=\frac{1}{2}$	$I=\frac{3}{2}$
$\beta_2^{\rm lin}$	0.43 ± 0.02	0.30 ± 0.03	0.34 ± 0.03	0.53	0.48	0.48 ± 0.04
$\beta_4^{\rm lin}$	−1.09 ± 0.04	−0.43 ± 0.03	−0.50 ± 0.04	−1.09	−0.41	−0.42 ± 0.04

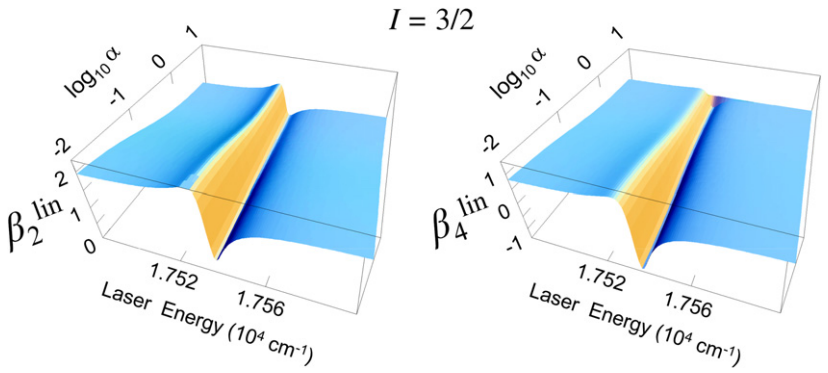

Figure 4. The predicted effect of the parameter $\alpha = (A/\Gamma)^2$ on the profiles of the $\beta_2^{\rm lin}$ and $\beta_4^{\rm lin}$ parameters for the ^{131}Xe isotope with $I=\frac{3}{2}$.

are missing. Despite this, as can be seen from panels (c)–(f) of figure 3, the agreement between theory and experiment for the isotopes with nonzero spin is almost as good as for the isotopes with $I=0$.

The results for the asymmetry parameters for the latter isotopes should be automatically consistent once the depolarization factors due to the coupling between the electronic and nuclear angular momenta are properly included. As can be seen from panels (c)–(f) of figure 3 this is generally the case.

The intervals of variation of $\beta_k^{\rm lin}$ $(k=2,\ 4)$ across the resonance are approximately similar for the isotopes with $I=\frac{1}{2}$ and $I=\frac{3}{2}$ and are smaller than for the isotopes with $I=0$ in accordance with the depolarization factors discussed in the previous section. Using the depolarization factors found above for the ^{131}Xe isotope from the data on CD improves the agreement between theory and measurements (panels (e) and (f)).

Table 2 presents data at the resonance energy E_r for the cross section. As one can see from this table, where the experiment and theory are compared in a quantitative manner, the asymmetry parameters for the ^{131}Xe $(I=\frac{3}{2})$ isotope are larger than for ^{129}Xe $(I=\frac{1}{2})$ which could initially be associated with higher alignment for the former isotope. In fact, the alignments are almost equal, but because the depolarization affects both nominator and denominator of (17) and (18), the observed asymmetry parameters are higher for the $I=\frac{3}{2}$ isotope. The error bars in the last column of table 2 are due to the fact that we have used experimental data to estimate the influence of the HFS. Note that the profiles for $\beta_k^{\rm lin}$ $(k=2,\ 4)$ for all isotopes are equally broadened and shifted with respect to the profile of the resonance in the angle-integrated cross section in accordance with the scaling theorem [37].

To further illustrate the sensitivity of the asymmetry parameters to the HFS interaction, figure 4 presents the resonance profiles of $\beta_2^{\rm lin}$ and $\beta_4^{\rm lin}$ as functions of the parameter α for the isotope with $I=\frac{3}{2}$. Generally the influence is large. Note that the 'weak' channels with $J=0,\ 1$ strongly influence the parameter $\beta_2^{\rm lin}$ for all values of α (left panel), while their effect on $\beta_4^{\rm lin}$ are restricted by the low values of α (right panel).

Figure 5 presents our results for the circularly polarized beams. In this case we measured PADs only at the resonant energy E_r. The 'weak' channels with $J=0,\ 1$ are not excited for the isotope with $I=0$ (i.e. without the depolarization) for the beams with parallel photon spins due to the selection rules for the magnetic quantum number. Therefore only β_2^{+-} and β_4^{+-} are changed by inclusion of the 'weak' channels and their influence is crucial (panels (a) and (b)). The resonance behavior of the β_2 parameter changes completely, turning from the window-type to the resonance-type. The agreement between theory and measurements is good. For the ^{131}Xe isotope, the depolarization coefficients found above from the analysis of the CD data, lead to slightly better agreement between theory and experiment than in the case of assumption of the separated HFS levels (panels (e) and (f)).

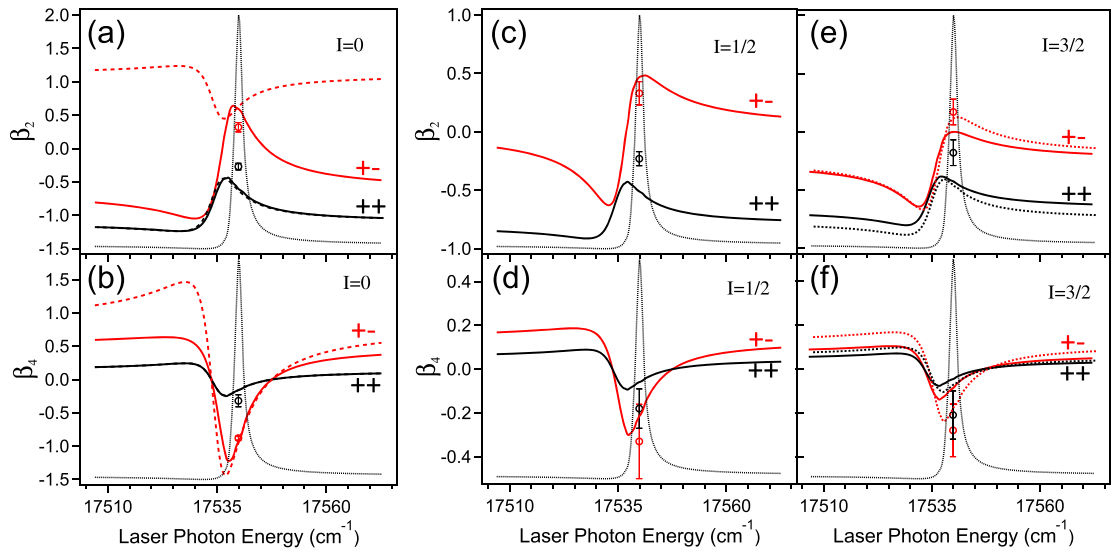

Figure 5. The β_2^{++} and β_2^{+-} (top) and β_4^{++} and β_4^{+-} (bottom) parameters for Xe ions with nuclear spin $I = 0$ (panels (a) and (b)), $I = \frac{1}{2}$ (panels (c) and (d)), and $I = \frac{3}{2}$ (panels (e) and (f)) at different laser wavelengths across the $5d[\frac{3}{2}]_1 + \gamma_{las} \rightarrow 4f'[\frac{5}{2}]_2$ resonance. The experimental data for the resonance energy E_r (open circle) are extracted from the VMI images recorded in coincidence with the corresponding isotopes. MCHF calculations: red lines, β_2^{+-} and β_4^{+-}; black lines, β_2^{++} and β_4^{++}. Dashed lines: MCHF with only resonant channels $J = 2$. Solid lines: MCHF with $\alpha \gg 1$. In panels (e) and (f): dotted lines are for the case of α extracted from the CD measurements. The profile of the $4f'[\frac{5}{2}]_2$ resonance in the angle-integrated cross section σ is shown for comparison (dotted line).

5. Conclusions

We considered, both experimentally and theoretically, isotopically resolved two-photon two-color resonant ionization of atoms by circularly and linearly polarized light beams, when first an intermediate atomic state is photoexcited and then further ionized in the region of an autoionizing resonance. Particular results have been obtained for the Xe isotopes with the nuclear spin 0, $\frac{1}{2}$ and $\frac{3}{2}$, which were ionized in the region of the autoionizing state $5p^5(^2P_{1/2})4f[\frac{5}{2}]_2$ via excitation of the intermediate $5p^5(^2P_{3/2})5d[\frac{3}{2}]_1$ state. The PADs and dichroism show high sensitivity with respect to the isotope because of depolarization of the intermediate excited state due to the hyperfine interactions between the electron cloud and magnetic moment of the nucleus. It is remarkable that a tiny hyperfine interaction can cause quite pronounced effects on a pure atomic process. Good agreement between extensive multiconfiguration calculations and experimental data were achieved. We were able to estimate a previously unknown HFS constant for a case of not isolated HFS levels.

Acknowledgments

We thank the general technical SOLEIL staff for smoothly running the facility, and for the allocated beamtime under project 20100271. The experimental research reported here has received funding from the European Community's Seventh Framework Programme (FP7/2007-2013) under Grant Agreement No. 226716. EVG, ANG acknowledge support by the Russian Foundation for Basic Research (RFBR) under grant 12-02-01123 and hospitality at the European XFEL (Hamburg, Germany), where a part of this work was done. EVG gratefully acknowledges financial support by the Dynasty Foundation via the Support Program for Young Scientists. MM acknowledges support by the Deutsche Forschungsgemeinschaft (DFG) under grant no. SFB 925/A1.

References

[1] Wuilleumier F and Meyer M 2006 *J. Phys.* B **39** 425–77
[2] Kleinpoppen H, Lohmann B and Grum-Grzhimailo A N 2013 *Perfect/Complete Scattering Experiments. Probing Quantum Mechanics on Atomic and Molecular Collisions and Coincidences* (Berlin: Springer)
[3] Haroche S, Paisner J A and Schawlow A L 1973 *Phys. Rev. Lett.* **30** 948–51
[4] Fano U and Macek J H 1973 *Rev. Mod. Phys.* **45** 553–73
[5] Greene C H and Zare R N 1982 *Phys. Rev.* A **25** 2031–7
[6] Strand M P, Hansen J, Chien R L and Berry R 1978 *Chem. Phys. Lett.* **59** 205–9
[7] Hansen J C, Duncanson J A, Chien R L and Berry R S 1980 *Phys. Rev.* A **21** 222–33
[8] Chien R, Mullins O C and Berry R S 1983 *Phys. Rev.* A **28** 2078–84

[9] Mullins O C, Chien R l, Hunter J E, Keller J S and Berry R S 1985 *Phys. Rev.* A **31** 321–8
[10] Compton R N, Stockdale J A D, Cooper C D, Tang X and Lambropoulos P 1984 *Phys. Rev.* A **30** 1766–74
[11] Kaminski H, Kessler J and Kollath K J 1980 *Phys. Rev. Lett.* **45** 1161–4
[12] Wörner H J, Grütter M, Vliegen E and Merkt F 2005 *Phys. Rev.* A **71** 052504
[13] O'Keeffe P, Gryzlova E V, Cubaynes D, Garcia G A, Nahon L, Grum-Grzhimailo A N and Meyer M 2013 *Phys. Rev. Lett.* **111** 243002
[14] Nahon L, de Oliveira N, Garcia G A, Gil J F, Pilette B, Marcouille O, Lagarde B and Polack F 2012 *J. Synchrotron Radiat.* **19** 508–20
[15] Marcouille O, Brunelle P, Chubar O, Marteau F, Massal M, Nahon L, Tavakoli K, Veteran J and Filhol J 2007 *AIP Conf. Proc.* **879** 311–4
[16] Mercier B, Compin M, Prevost C, Bellec G, Thissen R, Dutuit O and Nahon L 2000 *J. Vac. Sci. Technol.* A **18** 2533–41
[17] Nahon L and Alcaraz C 2004 *Appl. Opt.* **43** 1024–37
[18] Garcia G A, Soldi-Lose H and Nahon L 2009 *Rev. Sci. Instrum.* **80** 023102
[19] Céolin D, Chaplier G, Lemonnier M, Garcia G A, Miron C, Nahon L, Simon M, Leclercq N and Morin P 2005 *Rev. Sci. Instrum.* **76** 043302
[20] Garcia G A, Nahon L and Powis I 2004 *Rev. Sci. Instrum.* **75** 4989–96
[21] Balashov V V, Grum-Grzhimailo A N and Kabachnik N M 2000 *Polarization and Correlation Phenomena in Atomic Collisions. A Practical Theory Course* (New York: Plenum)
[22] Baier S, Grum-Grzhimailo A N and Kabachnik N M 1994 *J. Phys. B: At. Mol. Opt. Phys.* **27** 3363–88
[23] Kabachnik N M and Sazhina I P 1976 *J. Phys. B: At. Mol. Opt. Phys.* **9** 1681–97
[24] Fischer C F, Brage T and Jönsson P 1997 *Computational Atomic Structure. An MCHF Approach* (Bristol: Institute of Physics Publishing)
[25] Meyer M, Gisselbrecht M, Marquette A, Delisle C, Larzillière M, Petrov I D, Demekhina N V and Sukhorukov V L 2005 *J. Phys. B: At. Mol. Opt. Phys.* **38** 285–95
[26] Gisselbrecht M, Marquette A and Meyer M 1998 *J. Phys. B: At. Mol. Opt. Phys.* **31** 977–84
[27] King R F and Latimer C J 1982 *J. Opt. Soc. Am.* **72** 306–8
[28] Petrov I D, Peters T, Halfmann T, Aloïse S, O'Keeffe P, Meyer M, Sukhorukov V L and Hotop H 2006 *Eur. Phys. J. D—At. Mol. Opt. Plasma Phys.* **40** 181–93
[29] Liberman S 1969 *J. Phys.* **30** 53–62
[30] Liberman S 1971 *J. Phys.* **32** 867–70
[31] Luc-Koenig E 1972 *J. Phys.* **33** 847–52
[32] Prior M H and Johnson C E 1972 *Phys. Rev.* A **5** 550–6
[33] Jackson D A and Coulombe M C 1972 *Proc. R. Soc.* A **327** 137–45
[34] Geisen H, Krümpelmann T, Neuschäfer D and Ottinger C 1988 *Phys. Lett.* A **130** 299–304
[35] Pawelec E, Mazouffre S and Sadeghi N 2011 *Spectrochim. Acta* B **66** 470–5
[36] Chan W F, Cooper G, Guo X, Burton G R and Brion C E 1992 *Phys. Rev.* A **46** 149–71
[37] Grum-Grzhimailo A N, Fritzsche S, O'Keeffe P and Meyer M 2005 *J. Phys. B: At. Mol. Opt. Phys.* **38** 2545–53